Journal of Computational Neuroscience, Vol. no. 9, Issue No. 1, 67–81 (2000)

Computational Consequences of Temporally Asymmetric Learning Rules: II. Sensory Image Cancellation

PATRICK D. ROBERTS AND CURTIS C. BELL

proberts@reed.edu

Neurological Sciences Institute, OHSU, 1120 N.W. 20th Avenue, Portland, OR 97209

Received September 22, 1998; Revised August 4, 1999

Abstract. The electrosensory lateral line lobe (ELL) of mormyrid electric fish is a cerebellum-like structure that receives primary afferent input from electroreceptors in the skin. Purkinje-like cells in ELL store and retrieve a temporally precise negative image of prior sensory input. The stored image is derived from the association of centrally originating predictive signals with peripherally originating sensory input. The predictive signals are probably conveyed by parallel fibers. Recent *in vitro* experiments have demonstrated that pairing parallel fiber-evoked excitatory postsynaptic potentials (epsps) with postsynaptic spikes in Purkinje-like cells depresses the strength of these synapses. The depression has a tight dependence on the temporal order of pre- and postsynaptic events. The postsynaptic spike must follow the onset of the epsp within a window of about 60 msec for the depression to occur and pairings at other delays yield a non-associative enhancement of the epsp. Mathematical analyses and computer simulations are used here to test the hypothesis that synaptic plasticity of the type established *in vitro* could be responsible for the storage of temporal patterns that is observed *in vivo*. This hypothesis is confirmed. The temporally asymmetric learning rule established *in vitro* results in the storage of activity patterns as observed *in vivo*, and does so with significantly greater fidelity than other types of learning rules. The results demonstrate the importance of precise timing in pre- and postsynaptic activity for accurate storage of temporal information.

Keywords: synaptic plasticity, learning rule, electric fish, instability

1. Introduction

This article shows how synaptic plasticity in the electrosensory lateral line lobe (ELL) of mormyrid electric fish results in the storage of temporal information. Temporal information about sensory and motor signals must be stored in the central nervous system in order for the organism to profit from experience and to coordinate its motor activity. Much is known about the timing of sensory responses and motor signals, but the neural mechanisms that permit the storage of temporal information are not yet well characterized. In the mormyrid ELL, temporal information is stored through a process of adjusting the synaptic efficacy of temporally correlated signals that do not themselves encode the stored information.

The mormyrid ELL is one member of a class of cerebellum-like sensory structures that are found in fish, amphibia, and mammals (represented in

mammals by the dorsal cochlear nucleus). Several of these structures in fish have been shown to act as adaptive sensory processors in which predictions or expectations about sensory input are generated by an associative process and subtracted from actual sensory input, allowing unexpected input to stand out [Bastian, 1995, Bell et al., l997a, Bodznick et al., l992]. Thus, work on the mormyrid ELL is relevant to an entire class of structures. Furthermore, the mormyrid ELL and other cerebellum-like structures are similar enough to the cerebellum itself that understanding them could provide insight into cerebellar function.

Synaptic plasticity has been established in *in vitro* studies of the mormyrid ELL at the synapse between parallel fibers and Purkinje-like medium ganglion cells. This plasticity is associative and obeys a temporally asymmetric learning rule [Bell et al., l997a]. Depression of synaptic efficacy takes place after pairings in which the postsynaptic spike occurs within a short interval after the onset of the parallel fiber-evoked epsp. Enhancement of efficacy takes place after pairings at all other delays between the epsp and the postsynaptic spike. Asymmetric learning rules have also been observed in other systems [Bi and ming Poo, 1998, Levy and Steward, 1983, Markram et al., l997, Zhang et al., 1998]. In these other systems, however, occurrence of the postsynaptic spike within a short interval following epsp onset leads to enhancement of synaptic efficacy.

The mormyrid ELL presents a special opportunity for examining the storage of temporal information because of the plasticity that has been demonstrated at both the systems and synaptic levels. But the connection between these two levels is far from direct - between changes at single synapses and changes in responses to normal sensory and motor signals of whole neurons embedded in a circuit. Modeling studies, such as those presented here, can help bridge the gap between synaptic and systems levels.

This study shows that the *minimal* requirements for storing a negative image of prior sensory information in the mormyrid ELL are the temporally asymmetric learning rule that has been established *in vitro* and a series of delayed parallel fibers inputs that are time-locked to a reference moter command (see next section). The study also shows that the specific learning rule established in *in vitro* studies [Bell et al., l997b] is *optimal* for such storage.

More generally, the study indicates that subtle variations in the learning rule, that is, in the timing relations between pre- and postsynaptic events that induce synaptic change, lead to major differences in the large scale dynamics of neuronal responses. Different learning rules appear to have functional consequences that are useful for different neural computations.

The next subsection presents necessary biological background information about the mormyrid ELL. This is followed by a section describing our theoretical approach and its implementation in the simulations. The third section compares the results of the model to the physiological results.

Temporal information storage in electrosensory processing.
The mormyrid electric fish senses its environment by emitting an electric organ discharge (EOD) and detecting the perturbations that nearby objects cause in the self-generated electric field. Specialized *mormyromast* electroreceptors sense the self-generated field and its distortions. Other electrosensory organs, the *ampullary electroreceptors*, are used by the fish to detect low-frequency, externally generated electric fields. Afferent fibers from both types of electroreceptors respond to the fish's own electric organ discharge, and these responses are conveyed to the cortex of the ELL where the fibers terminate in separate mormyromast and ampullary zones. The present modeling study is concerned with only the ampullary region of the ELL cortex because cells of the ampullary zone show temporal storage more clearly than cells of the mormyromast zones.

The cortex of the ELL not only receives input from the periphery, but also receives electric organ corollary discharge (EOCD) signals from central structures. These EOCD signals are correlated in time with the motor command that elicits the electric organ discharge. The corollary discharge signals reach the ELL cortex via various pathways, of which the eminentia granularis posterior (EGp) is the most important for the present model (Fig. 1). EGp receives electric organ corollary discharge signals at various delays up to about 80 msec [Bell

et al., 1992] and additional delays within this pathway are probably also present. Axons of cells in the EGp form the parallel fibers of the ELL molecular layer. Thus, individual parallel fibers are believed to discharge at specific delays of zero to about 100 msec following each electric organ discharge. The net result is a series of signals at different delays in different parallel fibers. Other types of predictive signals besides the corollary discharge signals, such as proprioceptive and descending electrosensory signals, are probably also involved in adaptive processes [Bastian, 1995, Bell et al., 1997a, Bodznick et al., 1992], but only electric organ corollary discharge signals will be modeled in this study.

The objective of the present model is to study the adaptive responses of medium ganglion (MG) cells of the ELL. Parallel fibers synapse on the apical dendrites of MG cells, (Fig.1) in the molecular layer of the ELL. Basal dendrites of MG cells in the deeper layers receive electrosensory input from the periphery via excitatory or inhibitory interneurons. There are also efferent cells in the ELL (not shown in Fig.1) that are inhibited or excited by electrosensory stimuli in the centers of their receptive fields. Medium ganglion cells are inhibitory (GABAergic) Purkinje-like interneurons which synapse locally on the efferent cells and on each other. Only the Purkinje-like MG cells are modeled in the present study, as these are the most numerous cell type receiving both parallel fiber input on apical dendrites and electrosensory input on basal dendrites. In addition, MG cells show greater synaptic plasticity than the similarly situated efferent cells (Bell, unpublished observation).

Extra- and intracellular recording *in vivo* has shown that the responses of MG cells to the electric organ motor command are plastic [Bell, 1982, Bell et al., 1993]. Pairing the electric organ command signal with an electrosensory stimulus for a few minutes results in the development of a response to the command alone that is a negative image of the previously paired response to the sensory stimulus [Bell and Szabo, 1986] (see Fig. 2). The negative image is a kind of prediction about expected sensory input that is specific to the time course of the sensory response (which lasts about 100 msec in the ampullary region) and its polarity (excitation or inhibition). In the ampullary zone, the addition of a negative image of expected input to the actual input minimizes a potentially disruptive input due to the fish's own electric organ discharge.

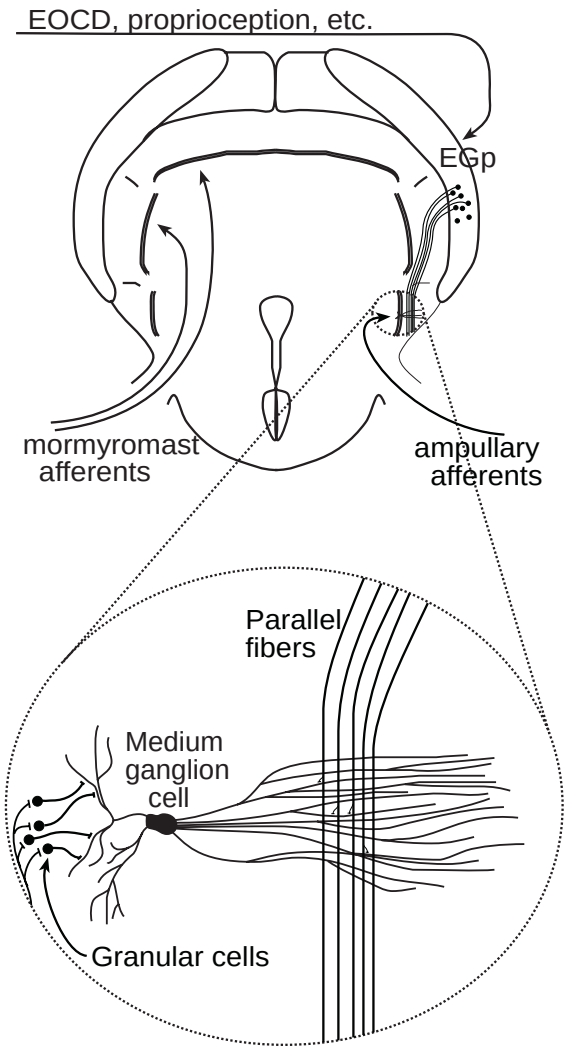

Fig. 1. Connectivity of the ELL. Parallel fibers arise from cells in the eminentia granularis posterior (EGp) and have synapses on the apical molecular layer dendrites of medium ganglion cells (MG) in the ELL. Primary afferent fibers from electroreceptors terminate on granular neurons in the deeper layers of the ELL and the granular neurons in turn relay electrosensory input to the basal dendrites of medium ganglion cells.

A combination of observations have lead to the hypothesis that the generation of negative images is due to anti-Hebbian synaptic plasticity at the synapse between parallel fibers and apical

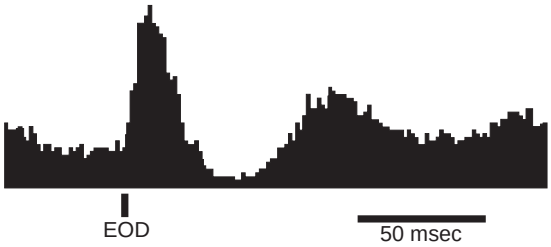

Fig. 2. Electrosensory afferent input from ampullary receptors. Histogram of a typical ampullary afferent fiber response following an electric organ discharge (1 msec bins) (modified from Bell and Szabo, 1986).

dendrites of medium ganglion and efferent cells. The hypothesis is that pairing electrosensory input to the basilar dendrites of medium ganglion cells with EOCD-linked parallel fiber input to the apical dendrites leads to a reduction of synaptic efficacy at paired synapses. Reduction of efficacy at these paired parallel fiber synapses, relative to other parallel fiber synapses, results in the formation of an EOCD-driven negative image of the previously associated electrosensory input.

The hypothesis that the generation of negative images as observed *in vivo* is due to anti-Hebbian plasticity at the synapses from parallel fibers onto MG cells has been strengthened by the demonstration of such plasticity in the *in vitro* slice preparation [Bell et al., 1997b]. MG cells show two types of spikes: a small, narrow, axon spike that does not invade the soma; and a large, broad soma-dendritic spike that probably propagates into the apical dendrites. The threshold of the large broad spike is 1.2 to 1.6 [Grant et al., 1998] times the threshold of the small spike. Associative plasticity in MG cells appears to be critically dependent on the broad spike as well as on the timing of this spike with respect to the parallel fiber epsp during pairing. [Bell et al., 1993, Bell et al., 1997b] Depression of the epsp was observed only after pairings in which the broad spike was evoked between 0 and 60 msec after the onset of the parallel fiber epsp (Fig.3). Pairings at other delays yielded enhancement. The enhancement appeared to be mainly non-associative, although there was some suggestion of an associative enhancement after pairings in which the broad spike occurred just before the epsp.

Recent work has shown that the associative depression at the parallel fiber synapse is blocked by the NMDA receptor antagonist AP5 [Han et al., 1999]. This involvement of the NMDA receptor explains the temporal asymmetry of the learning rule [Abbott and Blum, 1996, Gerstner et al., 1993, Levy and Steward, 1983]. Presumably, the plasticity requires calcium entry through NMDA channels, and this takes place only when the postsynaptic depolarization, caused by the broad spike, occurs during the binding of glutamate to the NMDA receptor

Although it is clear that synaptic plasticity is responsible for temporal information storage, it is not clear how the neural circuitry interacts with the single synapse learning rule measured *in vitro*

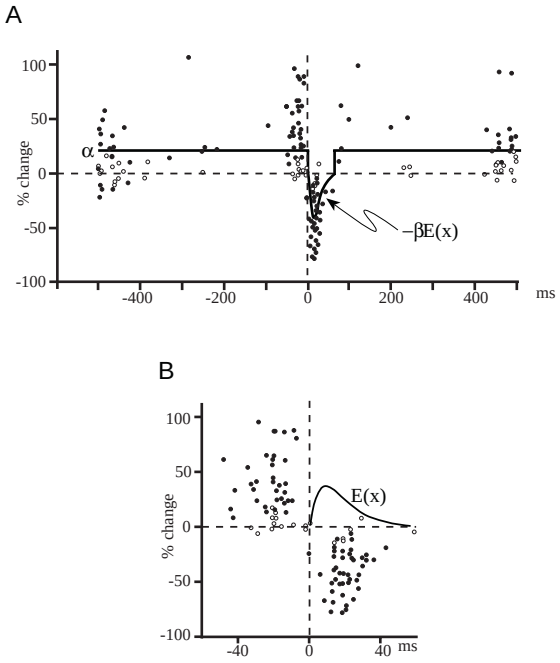

Fig. 3. Synaptic change due to pairing of broad spikes with epsps (A) Modified figure from (Bell et al., 1997c) showing percent change in epsp amplitude as a function of delay between onset of epsp and broad spike peak. Open circles represent changes that were not statistically significant. The curve represents the physiological learning rule investigated in the analytic section of the results. The model rule consists of a flat segment determined by non-associative learning rate, α, and an associative segment given by the product of the associative learning rate, β, and the epsp waveform, $E(x)$. (B) Center 100 msec of (A) with superimposed epsp waveform.

to accomplish the accurate storage and retrieval of temporal information. The only model of a similar electrosensory system is in elasmobranchs [Nelson and Paulin, 1995]. In that model, the learning rules of synaptic plasticity were introduced *ad hoc* to insure convergence because there was little physiological data available at that time. Now that the biological learning rule in the ELL is well characterized [Bell et al., 1997b], we may refine our understanding about aspects of the ELL that influence the accuracy of its stored image. In the following, a model of the ELL is constructed so that mathematical analyses and computer simulations may be used to evaluate the influence of different ELL properties on the storage of temporal information.

2. Methods

Both analytic and simulation methods were used to address the specific problem of whether the temporal learning rule that is observed *in vitro* is consistent with the generation of a negative image in ELL as observed *in vivo*. The analytic approach used a *stochastic* modeling technique to capture the physiological facts presented above in a mathematical formalism that is valuable for characterizing neuronal activity through time. The model neuron representing the MG cell is influenced by noise so that we are able to compute time-averages of the spike frequency. However, it will be seen that MG cells in the ampullary region of the ELL exhibit both a frequency coded output, plus a pulse coding to regulate synaptic plasticity. Both of these coding schemes are equally well represented in the model.

The results of the analytic component of this study are compared with computer simulations as a non-trivial check on the functional relations between averages of variables. The simulation of the time evolution of spike probability functions is carried out with a *Monte Carlo simulation* [Binder, 1979]. The simulation takes advantage of the stochastic nature of noisy neural systems to estimate the behavior in a computationally efficient implementation of the model. Additional features of the system are also demonstrated with the simulations in addition to verifying the hypothesis that the measured temporal learning rule is responsible for the negative image.

The goal of the model is to analyze the time-dependent activity of medium ganglion cells in the ampullary region of the ELL. The anatomical connectivity represented in Fig. 4A identifies the chief elements of the model. At every electric organ discharge, a sequence of epsps arrives at the apical dendrites via parallel fibers, while the ampullary fiber inputs from the periphery arrive at the basilar dendrites (Fig.4B). Each epsp is evoked at a characteristic delay between 0 and 100 msec following the electric organ command.

2.1 Stochastic model of the ELL.
In the experiments that are modeled [Bell, 1982], the EOD-stimulation cycle was about 1 Hz, and it is evident from recent experiments [Bell et al., 1997b] that significant changes in synaptic strength require many electric organ discharge cycles. The spike rate, on the other hand, has its greatest modulation *during* each cycle. Thus, the representation of time will be broken into cycles parametrized by two variables, (x,t), where x denotes the time following each electric organ command, and t represents the number of EOD cycles. This separation of the independent variables into different time courses is reminiscent of previous studies using multi-level analysis [Chauvet, 1993] to incorporate different time scales in neural models. The fast variable, x, is discretized in time steps of $\triangle x$, and we write $x_n = n(\triangle x)$.

The output of the medium ganglion cell will be represented by two spike probability functions. The broad spike probability function, $f_b(x,t)$, quantifies the probability of a *broad* spike at x milliseconds following an electric organ command signal issued at time t. There is an analogous spike probability for *narrow* spikes. Although the narrow spikes propagate via the axon to other neurons and are thus the carriers of information, we will focus on the broad spikes because they are most important for the learning dynamics of the system. In the simulations, it is convenient to include narrow spike output for comparisons with experimental results. The spike probability functions are modeled as being dependent on the *average* membrane potential, $\bar{V}(x,t)$, which is modified by synaptic input. The stochastic aspect of the model is represented by a parameter that

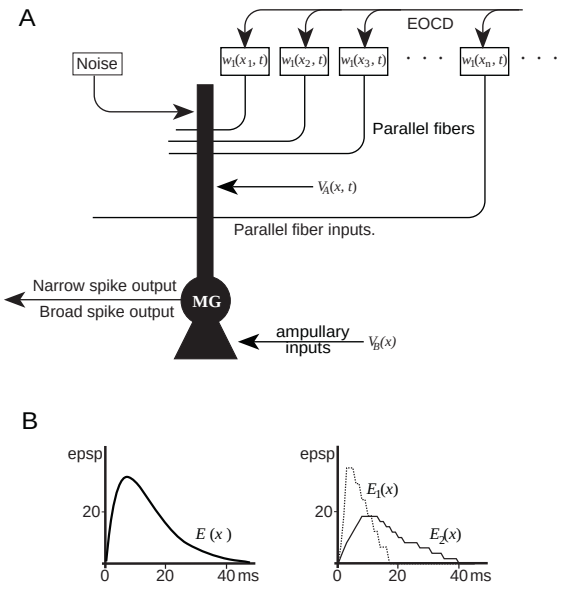

Fig. 4. Model of an ELL medium ganglion cell (A) Schematic diagram of MG cell model. The model MG cell receives inputs from a time delay series of weighted epsps ($V_A(x,t)$) and electrosensory input from ampullary electroreceptors ($V_B(x)$). The model calculates the response of the neuron to the electric organ discharge, ie. the responses to the sensory input which does not change during a learning sequence and the responses to the EOCD correlated parallel fiber activity which do change. All other synaptic inputs are absorbed into a noise term (see text for details). (B) Waveforms of epsps used in the analyses and simulations. In the analytic results, the epsps are represented as an alpha-function shown on the left, and in the simulations, two epsp waveforms are applied at each time-step, shown on the right.

quantifies the ambient noise, μ, in the membrane potential. The noise includes epsps that have no consistent temporal relationship with the EOCD signal, in addition to channel and membrane noise.

The stochastic representation is implemented by considering the membrane potential, V, as a random variable with a normal (Gaussian) distribution function centered about the average membrane potential, $\bar{V}(x,t)$. The probability of a spike in $\triangle x$ is represented by a sigmoidal function of the average membrane potential, centered about the broad spike threshold, θ_b,

$$f_b(x,t) = \frac{1}{1+\exp[-\mu(\bar{V}(x,t)-\theta_b)]}, \qquad (1)$$

where μ is a parameter related to the noise in the system. This expression defines the broad spike probability function by computing the probability that the membrane potential is greater than the threshold. A lower threshold value is used for computing the probability of narrow spikes.

The average membrane potential of the model ganglion cell is modulated by the sum of two sources of synaptic input, the basilar dendrites and the apical dendrites. The contribution of the basilar dendrites arises from primary afferents of the ampullary electroreceptors. These afferent signals are represented as a function, $V_B(x)$, that is the same for each EOD cycle during the learning sequence. Due to inhibitory interneurons in the deep layers of the ELL, the afferent signal shown in Fig. 2 is often inverted in the MG cells, as in the simulations.

The apical dendrites contribute a weighted sum of epsps that arise from parallel fiber signals originating in the EGp. The waveform of each epsp (shown in Fig. 4B) is represented by $E_i(x)$, where x represents the time that the parallel fiber impulse first reaches the synapse, and the index i classifies different time courses. These functions are normalized so that their integrals over one cycle are unity, $\sum_n E_i(x_n) = 1$, and when multiplied by a weighting factor, $w_i(x,t)$, yield the epsp. At each time step in the x-component ($x_n = n(\triangle x)$ with n an integer) up to the 100 msec limit for temporally correlated EOCD inputs, we assign synapses where the value of their epsps are equal to $w_i(x_n,t)E_i(x-x_n)$. The contribution to the membrane potential by the apical dendrites is then computed to be the linear sum of all epsps,

$$V_A(x,t) = \sum_i \sum_{n=1}^{N} w_i(x_n,t)E_i(x-x_n). \qquad (2)$$

where N represents the limit of temporally correlated input, and i is summed over the number of different epsp waveforms in the model.

This method of handling synaptic inputs is a modified version of the *spike response* model [Gerstner and van Hemmen, 1992]. The method is similar to the integrate-and-fire approach, but is a more biologically realistic representation of synaptic input on the membrane potential as measured at the soma. The most important difference between this approach and integrate-and-fire models

is the absence of an explicit refractory period in the spike generation function. Since we interpret the spike probability as the spike generator, the instantaneous broad spike frequency, ν_b, is computed by multiplying the probability function by the maximum frequency represented by the inverse of the refractory period, $\nu_b = (1/r_b) f_b(x,t)$. This modification of previous approaches greatly simplifies the analysis to allow a derivation of relevant functional relations between variables. To check the validity of this simplification, physiologically realistic refractory periods are included in the simulations.

The *in vitro* studies presented in [Bell et al., l997b] show that the learning rule for synaptic change has two components: non-associative enhancement and associative depression. The non-associative enhancement occurs whenever a synapse is active, regardless of the postsynaptic activity. Since each parallel fiber synapse is active once during the cycle, the enhancement will be represented as a constant weight change. The form of the associative depression learning window is represented by a function, $L_i(x)$. In keeping with experimental results, this function vanishes for values of x that are not in the interval, $0 \leq x \leq 60$ msec. The learning rule is formalized so that: if x_b represents the time a broad spike follows the onset of the EOD cycle, then the learning rule for each synaptic weight at time t that begins its associated epsp at x_n is

$$\triangle w_i(x_n,t) = \alpha - \beta L_i(x_b - x_n) \qquad (3)$$

where α determines the non-associative learning rate and β determines the associative learning rate for each synapse with an impulse arriving at $x = x_n$. The presence of a non-associative term implies that all of the synapses would saturate at their greatest values unless the average contribution of the associative depression is negative. Thus, we will normalize the associative learning function $\sum_n L_i(x_n) = 1$ and absorb the scale into β.

To analyze whether this learning rule combines with the model's anatomy to generate a stable negative image of the afferent input, we average the change in each synaptic weight per cycle, $\triangle w_n(t) = w_n(t+1) - w_n(t)$. The average change in synaptic weight is computed by using the broad spike probability function $f_b(x,t)$ and integrating over the cycle length:

$$< \triangle w_i(x_n,t) > \; = \; \alpha T - \beta \sum_m L_i(x_m - x_n) f_b(x_m,t), \quad (4)$$

where T is the cycle length and we will set $T = 1$ in the following analysis. This expression will be used to compute the average change in spike output of MG cells as a result of synaptic plasticity.

2.2 Simulations of MG cell activity.
The studies presented here are based on computer simulations of the ELL model shown in Fig. 4. Custom simulation software was written in C++ and a graphical user interface was designed using the Metrowerks Codewarrior compiler and libraries. The software used in this simulation can be obtained by anonymous FTP from `reed.edu/reed/users/proberts`.

A time-step of 1 msec in the x-component is used, and periodic boundary conditions are closed at 150 msec. This post-EOD time period is adequate because the maximum response time of the ampullary fibers is 100 msec so there could be no interference with the beginning of the EOD cycle. Each time step in the t-coordinate is counted as a single EOD-stimulus cycle.

There are 300 apical epsps in the simulation (2 at each of the 150 different delays, 1 msec apart) with temporally correlated signals tagged by the arrival time of the signal to the synapse at the apical dendrites. The 2 epsp inputs at each delay are of different waveforms, $E_1(x)$ and $E_2(x)$ shown in Fig. 4B, to simulate the possibility of different synaptic time courses. Two weights (one for each synapse) are associated with each time-step in the x-coordinate, and the weight saturation cutoffs are set at $1 \leq w \leq 60$.

The contribution to the membrane potential by the apical dendrites, $V_A(x,t)$, is computed using the expression in Eq.(2). The contribution by the basilar dendrites, $V_B(x,t)$, is set to mimic ampullary afferent fiber activity (Fig. 2) inverted by an inhibitory interneuron.

The sequence that the program executes during each EOD-stimulus cycle is as follows: First the modulation of the membrane potential due to the apical and basilar dendrites is computed. Next, a broad and/or narrow spike is assigned to each time step in the x-coordinate in accordance with a lin-

earized probability function. Finally, the synaptic weights are updated by scanning the region around a specific temporally correlated parallel fiber input for a broad spike within the range of its associative learning function, $L_i(x)$. A different learning function ($L_1(x)$ and $L_2(x)$) is associated with each epsp waveform ($E_1(x)$ and $E_2(x)$). If a broad spike is found then the synaptic weight is changed by an amount proportional to $L_i(x)$ (see Eq.(3)). Otherwise the weight is increased by the non-associative enhancement rate. The sequence is then iterated until terminated by the investigator.

3. Results

We wish to compute the final level of activity for the case in which the broad spike probability function $f_b(x,t)$ relaxes to a constant value over x due to pairing with the ampullary afferent signal [Bell, 1982]. In this model of the ELL, a high membrane potential at any time x increases the probability of broad spikes which in turn leads to synaptic depression. On the other hand, a low membrane potential leads to few broad spikes and non-associative plasticity increases the strengths of the corresponding synapses. Thus, there is a balance between these two types of plasticity that determines both the narrow and the broad spike frequencies.

The parallel fiber evoked epsp is depressed when the postsynaptic broad spike occurs within about 60 msec of epsp onset [Bell et al., 1997b]. This is about the same duration as the epsp itself, and we will show that this correspondence is essential for the formation of a faithful negative image of the ampullary input. This correspondence between the epsp and the learning rule makes sense computationally under the hypothesis that associative depression alters only those epsps that directly contribute to the generation of a postsynaptic broad spike. In the analytic portion of this investigation, we analyze the dynamics of the physiological learning rule [Bell et al., 1997b]. In the simulations, we make comparisons to variations on the learning rule and simulate the effects on the accuracy of the negative image.

3.1 Analytic results from the stochastic model of the ELL.

Let us assume that the sensory input represented in the model by $V_B(x)$ is well behaved enough that there exists a set of weights $\{\bar{w}_n\}$, that cause the apical input to an MG cell to exactly cancel the variations of the afferent input. If the weights take on these specific values, then the sum of the epsps with the afferent input, $V_B(x)$, will be constant:

$$\sum_{n \leq N} \bar{w}_n E(x - x_n) + V_B(x) = \bar{U}. \qquad (5)$$

where $\bar{U}$ is a constant in both x and t. The constant $\bar{U}$ represents the final average membrane potential to which the MG cell settles after a learning sequence that pairs the corollary discharge signal with the electric organ discharge. The assumption that such a set of weights exists is physiologically realistic because the basilar inputs represented by $V_B(x)$ are themselves transmitted to the MG cell through a sum of postsynaptic potentials. In this equation, and in the following analysis, only one epsp waveform is considered at each t-step.

If the weights converge to the set $\{\bar{w}_n\}$ under the influence of plasticity, then $\bar{V}(x_n,t) = \bar{U}$ when $< \triangle w(x_n,t) >= 0$, for each x_n. A constant average membrane pontential also implies that the broad spike probability is constant over x and t, $f_b(x,t) = \bar{f}_b$. Using the equation (4) for the average change of the weights, we find that the solution for the stationary broad spike probability is $\bar{f}_b = \alpha/\beta$ for any choice of associative learning window. Because the probability function is always less than one, the existence of a stationary weight configuration implies that $\alpha < \beta$. This is true because the temporal learning rule (Eq.3) is represented as a difference between enhancement and depression, and the associative depression must outweigh the ever-present non-associative enhancement.

If we substitute the apical contribution to the membrane potential from Eq.(5), $V_A(x,t) = \bar{U} - V_B(x)$, into the spike probability function, Eq.(1), we can solve for the stationary average membrane

potential:

$$\bar{U} = \theta_b - \frac{1}{\mu}\ln(\bar{f}_b^{-1} - 1) \tag{6}$$

Since $\bar{f}_b = \alpha/\beta$, this expression shows that the membrane potential in the stationary weight configuration is dependent on the broad spike threshold, the noise, and the ratio of the learning rates.

We will now calculate the time constant for the convergence to a stable negative image. The method is to expand the broad spike probability function about $\bar{V}(x,t) = \bar{U}$, and substitute this expression into the equation of the average change of the synaptic weights (Eq.4) in the continuous time (t) limit. Expanding the expression for the broad spike probability function (Eq.1) yields,

$$\begin{aligned} f_b(x,t) \; &= \\ &= \bar{f}_b + (\bar{V}(x,t) - \bar{U})\frac{\partial}{\partial \bar{V}} f_b(x,t)|_{\bar{V}=\bar{U}} + \cdots \\ &= \frac{\alpha}{\beta} + \mu\frac{\alpha}{\beta}(1 - \frac{\alpha}{\beta})(\bar{V}(x,t) - \bar{U}) + \cdots \end{aligned} \tag{7}$$

We now substitute this expression into Eq.(4) and take the continuum limit to obtain

$$\begin{aligned} \frac{d}{dt} < w(x_n,t) > \; &= \\ &= -\mu\alpha(1 - \frac{\alpha}{\beta}) \int L(x_n - x)(\bar{V}(x,t) - \bar{U})dx \\ &= -\mu\alpha(1 - \frac{\alpha}{\beta}) \int L(x_n - x) \times \\ &\times \sum_m (< w(x_m,t) > - \bar{w}_m)E(x_m - x)dx . \end{aligned} \tag{8}$$

where we are now ignoring the higher order terms in $(\bar{V}(x,t) - \bar{U})$. Notice that the explicit non-associative term of the learning rule has been cancelled. This is because when the average membrane potential is near $\bar{U}$, the system is in an equilibrium between the effects of associative and non-associative influences.

Although a constant broad spike frequency is a valid solution to Eq.(8), there may be other solutions that can be decomposed into a sum of oscillatory instabilities. Instabilities will grow as a function of t, so we must derive an expression for the decay constant, τ that quantifies the rate of approach to a stable membrane potential. The sign of τ will signify whether the ocsillations decay, or are unstable and grow in time. Our approach is to introduce an infinite set of oscillatory solutions, or *modes*, into the dynamical expression for the average weights given by Eq.(8). Then the decay rate corresponding to each mode will be calculated. The oscillations are assumed to be on the time-scale of the x-component and encode the deviations from the target weight configuration, $\{\bar{w}_n\}$. Let k represent the frequency of each mode. We seek solutions of the form,

$$< w(x_n,t) >= \bar{w}_n + e^{ikx_i}e^{-t/\tau}. \tag{9}$$

Substituting this expression into Eq.(8), and approximating the summation with an integral, we change variables to arrive at

$$\frac{1}{\tau} = \mu\alpha(1 - \frac{\alpha}{\beta}) \int\int L(y-z)E(y)e^{ikz}dy\,dz. \tag{10}$$

By expressing both $E(x)$ and $L(x)$ as α-functions we may derive an expression for the decay constant, τ. We will investigate the case where the wave form of the learning rule exactly matches the epsp wavefrom. Let $E(x) = E^2 x\exp(-Ex)$ and $L(x) = E^2 x\exp(-Ex)$ for $x > 0$ and these functions vanish for $x \leq 0$. The expression for τ then becomes,

$$\frac{1}{\tau} = \mu\alpha(1 - \frac{\alpha}{\beta})\frac{E^4}{2(E^2 + k^2)^2}. \tag{11}$$

For disturbances with wavelengths longer than the epsp waveform, such as the normal ampullary input, this time constant can be approximated as, $2/\tau = \mu\alpha(1 - \alpha/\beta)$. Since the decay constant is positive as long as $\alpha < \beta$, then the approach of the system to a constant final membrane potential is a valid solution of the dynamical equation of synaptic change. This expression appears to be valid only for the physiological form of the learning rule as reported in [Bell et al., 1997b] as is demonstrated in the following subsection. It can be shown that instabilities may arise in the solutions of Eq. 8 when $L \neq E$, and in the case that the associative segment of learning rule does not match the waveform of the epsp. However, it can also be shown that for a small range of $L \leq E$, the negative image is stable [Roberts, 1999b] These instabilities ruin the fidelity of the negative image so that cancellation of the afferent input is incomplete.

This subsection has shown that when the waveform of the epsp matches the associative learning

rule, all deviations of the final membrane potential from a constant value over x are suppressed by synaptic plasticity. Thus, the learning rule measured *in vivo* leads to the exact cancellation of the fishes own electric discharge signal. In addition, we have found that the final spike frequency after the pairing of the corollary discharge input with afferent input is determined only by the learning rates (α and β). The next subsection will demonstrates these conclusions with computer simulations. The simulations will also demonstrate the growth of unstable modes when there is a mismatch between the epsp waveform and the associative learning function.

3.2 Simulations of electrosensory processing.
The simulations have confirmed that the best match with experimental results of sensory adaptation of MG cells in the ampullary region appears when the associative learning rule is set by the epsp, $L(x) = E(x)$. The comparison with experimental data [Bell, 1982] is given in Fig. 6. The raster plot shows the creation of a negative image of the electrosensory signal from a combination of the temporally correlated parallel fiber inputs. In this simulation, the threshold for narrow spikes was set at 45% of the maximum membrane potential's value, and for broad spikes, 70%.

This model duplicates the experimental results obtained *in vivo* with naturally occurring sensory and motor signals using the learning rule obtained from *in vitro* studies [Bell et al., 1997b]. The simulation therefore supports the hypothesis that synaptic plasticity at parallel fiber synapses is a major component involved in the generation of negative images in the ELL.

A more detailed representation of the final weight configuration and the final membrane potential $V(x,t)$ is shown for the simulation at $t = 200$ (Fig. 5). The magnitude of the weights are shown to slightly proceed the form of the apical contribution to the membrane potential, $V_A(x,t)$ because the epsps project into higher values of x beyond each weights timing label. The basilar contribution, $V_B(x,t)$, has been represented by a piecewise linear function in the simulation. Thus, there are small peaks and dips in the total membrane potential that could not be exactly cancelled by $V_A(x,t)$, such as at $x = 30$. However, in the biological system, such sharp corners do not exist, and the ampullary afferent input is smooth enough for exact cancellation.

The learning rule used in the simulation (Fig. 7A) that generated the raster plot of Fig. 6 appears to provide the *optimal* timing for associative depression and non-associative enhancement. We tested various modifications of the learning rule as shown in Fig. 7 (B, C, and D), none of which generated a negative image as accurately as A.

To measure the deviation from a constant membrane potential (in x), we computed the mean square contingency given by the expression,

$$\frac{\chi^2(t)}{N} = \frac{1}{N}\sum_{n=1}^{N}\frac{(V(x_n,t) - < V(t) >)^2}{< V(t) >}, \quad (12)$$

where $< V(t) >$ is the membrane potential at time t averaged over the EOD cycle, and N is the number of time-steps in x. This quantity appears to be quite sensitive for measuring the deviations from a constant membrane potential.

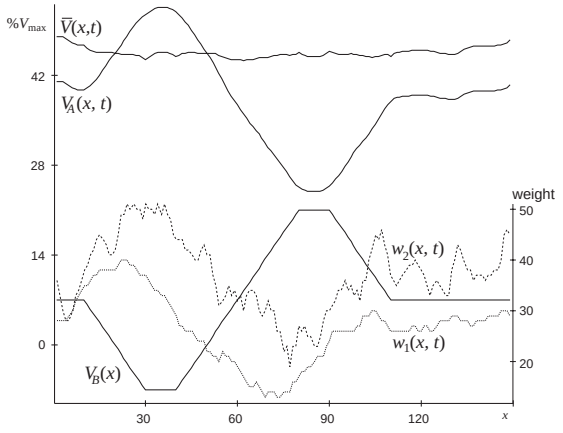

Fig. 5. Contribution of apical and basal inputs to generate the total membrane potential after pairing. The average total membrane potential, $\bar{V}(x,t)$, is simulated by adding the contribution of the basilar dendrites, $V_B(x,t)$, to the epsp waveforms multiplied by weighting factors, $w_1(x,t)$ and $w_2(x,t)$, that represent the contribution of the apical dendrites, $V_A(x,t)$. Thus, $V_A(x,t)$ is the "negative image" of the paired electrosensory input, $V_B(x,t)$ The noise in the weight traces is due to the stochastic assignment of broad spikes that drives the learning rule's associative component.

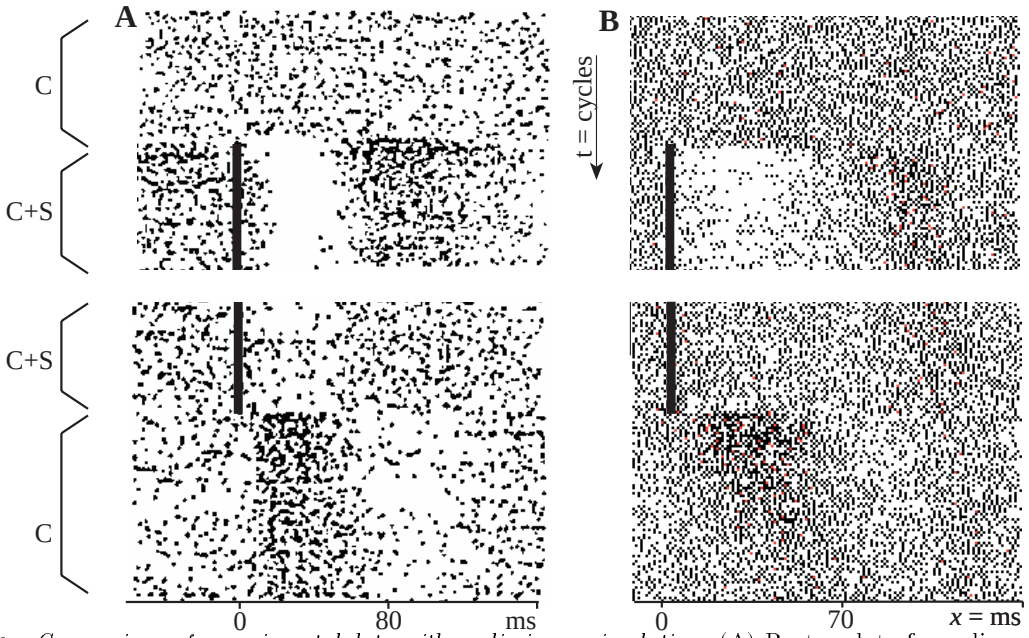

Fig. 6. Comparison of experimental data with preliminary simulation. (A) Raster plot of ganglion cell response from Bell, et al. (l997a). Each dot represents a spike and each row is an EOCD cycle. Command signal alone (C) yields no modulation of the cell activity. When an electrical stimulus is paired with the command (C+S), there is a pause followed by a burst. After 9 minutes of pairing, modulation subsides, and when the stimulus is silenced, a negative image is present, which eventually subsides. (B) Computer simulation of the same experimental paradigm as in (A) using the physiological learning rule.

The evolution of the mean square contingency is shown in Fig. 8. The same paradigm was used to generate this graph as in the raster plot of Fig. 6; the first phase simulated the stimulus plus command stimulus (C+S), then the stimulus was shut off (C) at $t = 100$. It can be seen that all of the learning rules show some adaptation that initially reduced the deviation from a constant potential. However, only the learning rule that most closely matches the physiological rule measured *in vitro* (A) reaches a mean square contingency of zero.

When the learning rule had no non-associative enhancement, all synapses eventually saturated at their minimal value. The physiological learning rule (A) with $\alpha = 0$ is able to reduce the total membrane potential when the sensory input ($V_b(x)$) is high, but cannot enhance the potential when the sensory input is low. The value of $\chi^2(t)/N$ simply freezes when the potential is reduced to a level where the noise cannot push the membrane potential over the threshold for broad spikes. In a simulation where the command signal was paired with sensory input for 400 EOD cycles, and $\chi^2(t)/N$ was recorded for 200 further cycles, the mean value was 17.0, with zero standard deviation because the membrane potential was below the level of broad spike generation. As a comparison, the same variable simulated with $\alpha = 1$ had a mean of 1.5 $\pm$0.9.

Distortions in the membrane potential were found when the learning rule was such that synaptic depression resulted from a symmetric associations within a small neighborhood of the beginning of an epsp (Fig. 7B), rather than from the requirement that the broad spike *follows* the onset of an epsp, as observed *in vitro* (Fig. 7A)). The symmetric association learning rule (Fig. 7B) generates a reasonably good negative image with a mean value for $\chi^2(t)/N$ equal to 17.0 $\pm$3.4 during the 200 EOD cycles following $t = 400$ (in comparison to 1.5 $\pm$0.9 for the learning rule found *in vitro* (Fig. 7A)). However, the dynamics of this learning rule are unstable so that oscillations in x begin to form after many cycles. For instance, when the simulation is allowed to run for 4000 EOD cycles, the mean value of $\chi^2(t)/N$ increases to 63.7 $\pm$15.7.

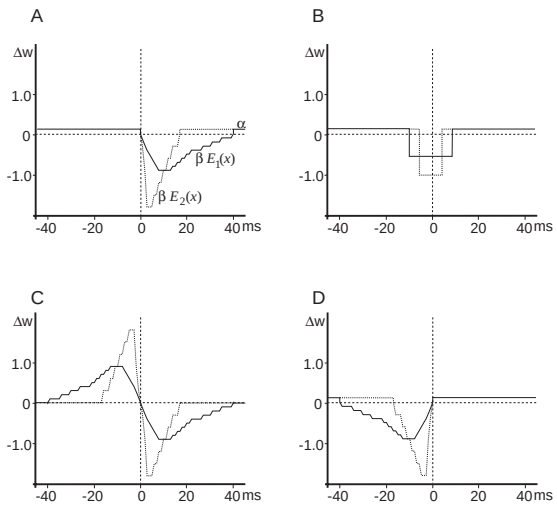

Fig. 7. Learning rules studied in the simulation (A) Learning rule that is consistent with data presented in (Bell et al. 1997b). (B) Temporally symmetric learning rule. (C) Temporally antisymmetric learning rule. (D) Learning where the associative depression is not coincident with the epsp.

The unstable oscillations are seen more clearly in the graph of the average membrane potential (Fig. 9). For each learning rule, the most unstable wavelength dominates the oscillations yielding the self-generated pattern. These oscillations represent unstable solutions to Eq.(8) discussed in the last section resulting from a negative decay constant.

Instabilities due to the dynamics of the learning rules become more apparent in the examples represented by Fig. 7C and D. The first rule (C) generates travelling waves in the x component similar to the instablilties analyzed in the companion paper [Roberts, 1999a]. This rule is opposite in sign to the physiological learning rule found in the neocortex [Markram et al., l997] in which epsp enhancement occurs when the postsynaptic spike followed the epsp onset by less than 100 msec and depression when the spike preceeded the epsp onset by less than 100 msec. The rule of Fig. 7C includes an associative enhancement for pairings when the broad spike immediately proceeds the epsp and no non-associative enhancement. Although the deviations from a constant membrane potential never grow very large, the system with this rule does not converge onto an accurate negative image. The mean value of the mean square contingency for the 200 EOD cycles following $t = 400$ is 68.3 $\pm$17.5. Since the integral of the associative portion of the rule is zero, a non-associative enhancement would cause an overall increase in the weights until they eventually saturate at their greatest values. Thus,

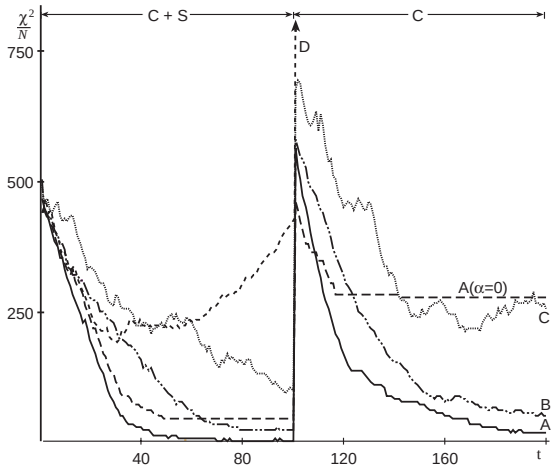

Fig. 8. Time evolution of adaptive response. The mean square contingency (defined in text) versus the number of EOD cycle for each of the learning rules of Fig. 7. For the first 100 EOD cycles, the command signal is paired with the sensory input (C+S), then the command cycle is presented alone (C). The letters identify the learning rule used in each simulation run.

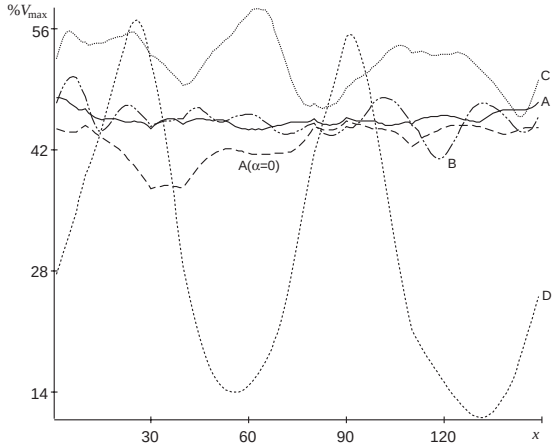

Fig. 9. Post-pairing membrane potentials for different learning rules. The average total membrane potential (arbitrary units) after pairing the command signal with sensory input for 450 EOD cycles (except for (D), which was paired for 400 cycles).

in this learning rule the non-associative enhancement was set to zero ($\alpha = 0$).

The most dramatic instabilities that were found in the simulations employing the learning rule represented by Fig. 7D where the associative depression is not coincident with the epsp. In this case, large stationary oscillations developed as seen in the "snap shot" of the membrane potential at $t = 400$ shown in Fig. 9. This kind of instability appears to be present in all learning rules when the associative depression is not coincident with the epsp waveform.

4. Discussion

The results presented in the previous section confirm that the necessary conditions for the ELL to generate a negative image to cancel the fish's own electric organ discharge are: (1) a series of delayed inputs that are correlated with the EOD, and (2) modifiability of parallel fiber synapses in accord with the learning rule shown in Fig. 3. Without the serial delayed inputs, there would be no time-ordered set of inputs from which to sculpt the negative image. In addition, learning rules that are different from the one demonstrated physiologically lead to suboptimal negative images and instabilities.

In *in vivo* experiments, pairing with a sensory stimulus that depolarized the MG cell led to a hyperpolarizing predictive response, and pairings with a hyperpolarizing sensory stimulus led to a depolarizing predictive response. Such symmetry was not observed, however, in pairings with intracellular current pulses. Pairings with depolarizing intracellular current pulses *in vitro* led to a hyperpolarizing predictive response (as in pairings with a sensory stimulus), but pairings with hyperpolarizing current pulses did not have any effect. Thus, on the cellular level pairing with postsynaptic depolarization, which causes a broad spike, leads to an associative synaptic depression, but pairing with postsynaptic hyperpolarization does not seem to cause any associative change in synaptic efficacy. This asymmetry was incorporated into the learning rule that was used in the model.

How then is the depolarizing predictive response following pairing with a hyperpolarizing sensory stimulus generated *in vivo* and in the model? In the model, the depolarizing predictive response is related to relative differences in the spontaneous activity of broad spikes. The depolarizing predictive response is generated because broad spikes are more likely to occur outside this period. Thus, on the average, parallel fiber epsps arriving during the hyperpolarization are less subject to associative depression than to non-associative enhancement. During the course of several EOD cycles, the parallel fiber epsps undergo a net increase in their contribution to the average membrane potential. In contrast, parallel fiber epsps arriving outside the period of hyperpolarization will be subject to relatively more associative depression due to the more frequent occurrence of broad spikes. The depolarizing predictive response in the model thus depends critically on the rate of occurrence of spontaneous broad spikes, which in turn depends on the amplitude and frequency of membrane potential *noise*. Spontaneous broad spikes are sometimes present in MG cells and such spikes could be part of the explanation for depolarizing predictive responses observed *in vivo*.

Another mechanism has also been suggested for explaining how a learning rule that allows associative changes in synaptic efficacy only after pairing with postsynaptic depolarizations could give rise to the symmetrical changes following pairing with excitatory and inhibitory sensory stimuli that are observed in vivo (Han et al. 1998). This explanation does not require spontaneous activity of broad spikes and relies on network elements that are present in the real ELL but not in the model. Two distinct types of medium ganglion cells are present in ELL, and the morphology suggests that one is an "on" cell, excited by sensory stimuli that excite primary afferent fiber, and the other is an "off" cell, inhibited by such sensory stimuli. Mutual inhibitory connections between two such MG cells could explain adaptive responses to depolarization even if synaptic plasticity only occurs after pairing with postsynaptic depolarization. Parallel fiber epsps onto the cell type that is depolarized by the sensory stimulus would be reduced by associative depression, but those on the MG cell type that is hyperpolarized by the same sensory stimulus would not change. Because of the plasticity, the cell paired with depolarization would show a pause after the pairing, disinhibiting the cell paired with hyperpolarization. The latter

would therefore give a burst response as a result of the pairing even though its synapses had not undergone any plastic change.

Another effect of mutual inhibition between opponent MG cells would be to equalize the rate of the adaptation to hyperpolarizing afferent input with the rate of adaptation to depolarizing afferent input, as is actually observed *in vivo* (unpublished observation). However, equality of adaptation rates is not a necessary consequence of the model. In fact, for the two rates to be the same in the model requires a precise and particular ratio between the associative and non-associative learning rates. Such a delicate balance seems unlikely in a biological system, and future studies will have to address this issue of equal adaptation rates.

The two components of the adaptive response, associative depression and non-associative enhancement, drive the spike output of MG cells to an equilibrium level that is determined by the ratio of the learning rates ($\alpha : \beta$ in Fig. 3). Thus, for any time interval within the first 100 msec following the electric organ discharge, deviations from the equilibrium spike output are damped. Since the average membrane potential is driven to the equilibrium level ($\bar{U}$ in Eq. 6), the learning rule will increase (decrease) the synaptic efficacy if the postsynaptic neuron is hyperpolarized (depolarized) from this level. In this respect, the learning rule of Fig. 3 is a biological implementation of the anti-*covariant* [Sejnowski, 1977] learning rule. However, random fluctuations that were reported by Sejnowski (1977) to result in cumulative errors, are, in the present case, an essential ingredient to the adaptive response of the MG neurons and lead to a reduction of errors.

Most temporal learning rules lead to instabilities, as illustrated in the simulations (Fig. 9, traces B, C, and D). In the present case, instabilities interfere with the functional role of the learning rule; the cancellation of predictable reafferent input. However, in some cases instabilities can be useful, as in the rule found in the mammalian cortex [Bi and ming Poo, 1998, Markram et al., 1997] that was studied in the companion paper [Roberts, 1999a]. In the cortical case, the circuitry takes advantage of the learning rule's dynamical instabilities to link associated events together in time. Thus, in the presently known biological temporal learning rules, one rule eliminates predictable sensory events to emphasize novel patterns, and the other induces a neuron to respond to a sensory event that is predictive of a future event. It will be interesting to discover if biological neural systems have developed other temporal learning rules for other functional uses, and how the function of these two known learning rules is affected by different neural architectures [Abbott and Blum, 1996, Gerstner et al., 1993].

It is instructive to compare the learning model presented here with other recent models of "spike-based" Hebbian learning [Gerstner et al., 1996, Kempter et al., 1999]. The model neurons are mathematically identical with the exception of a factor proportional to the noise in the linearized version of the present model's spike probability function (Eq.7). The main difference arises from how the separation of time scales is handled. In the present case, the fast time scale is assigned a separate coordinate, an approach that follows naturally from the experimental paradigm that is being modeled. In [Kempter et al., 1999], the equation of synaptic change is derived from a correlation of the pre- and postsynaptic spikes that is time averaged over the time interval of the learning trial. The result is a learning equation that does not convolve the learning function with the epsp waveform so that oscillatory instabilities found in the present analysis would be overlooked. This difference in formulation is important when the synaptic input is temporally correlated with a non-adaptive (background) input that represents the sensory image in the present case.

The exact timing of temporal learning rules has been shown here to result in important consequences for the dynamics of biological neural networks. The combination of analysis and simulations used here has illustrated these dynamics for the specific case of a single neuron responding to a delayed serial input correlated with a reference signal. This architecture is particularly relevant for the ELL which acts as an adaptive filter to cancel predictable reafferent input using corollary discharge information as a reference signal. The lessons learned in this system can be expected to have relevance to other similar neural systems as discussed in the introduction, and may form a basis for general principles of biological sensory processing.

Acknowledgements

The authors would like to thank Gin McCollum, Gerhard Magnus for discussions and helpful suggestions on the manuscript. This research was supported in part by a National Science Foundation grant (IBN 98-08887) awarded to PDR, by a National Science Foundation grant (IBN 98-96266) awarded to CCB, and by a National Institutes of Health grant (MH-49792) awarded to CCB.

References

[Abbott and Blum, 1996] Abbott, L. F. and Blum, K. I. (1996). Functional significance of long-term potentiation for sequence learning and prediction. *Cerebral Cortex*, 6:406–416.

[Bastian, 1995] Bastian, J. (1995). Pyramidal-cell plasticity in weakly electric fish: A mechanism for attenuating responses to reafferent electrosensory inputs. *J. Comp. Physiol. A*, 176:63–73.

[Bell, l982] Bell, C. C. (l982). Properties of a modifiable efference copy in an electric fish. *J. Neurophysiol.*, 47:1043–1056.

[Bell et al., l997a] Bell, C. C., Bodznick, D., Montgomery, J., and Bastian, J. (l997a). The generation and subtraction of sensory expectations within cerebellum-like structures. *Brain. Beh. Evol.*, 50:17–31. (suppl.1).

[Bell et al., l993] Bell, C. C., Caputi, A., Grant, K., and Serrier, J. (l993). Storage of a sensory pattern by anti-Hebbian synaptic plasticity in an electric fish. *Proc. Natl. Acad. Sci. USA*, 90:4650–4654.

[Bell et al., l992] Bell, C. C., Grant, K., and Serrier, J. (l992). Sensory processing and corollary discharge effects in the mormyromast regions of the mormyrid electrosensory lobe: I. Field potentials and cellular activity in associated structures. *J. Neurophysiol.*, 68:843–858.

[Bell et al., l997b] Bell, C. C., Han, V., Sugawara, Y., and Grant, K. (l997b). Synaptic plasticity in a cerebellum-like structure depends on temporal order. *Nature*, 387:278–281.

[Bell and Szabo, l986] Bell, C. C. and Szabo, T. (l986). Electroreception in mormyrid fish: Central anatomy. In Bullock, T. H. and Heiligenberg, W., editors, *Electroreception*, pages 375–421, New York. Wiley.

[Bi and ming Poo, 1998] Bi, Q. and ming Poo, M. (1998). Precise spike timing determines the direction and extent of synaptic modifications in cultured hippocampal neurons. *J. Neurosci.*, 18:10464–10472.

[Binder, l979] Binder, K. (l979). Introduction: Theory and "technical" aspects of Monte Carlo simulations. In Binder, K., editor, *Monte Carlo Methods in Statistical Physics*, pages 1–45, Berlin. Springer-Verlag.

[Bodznick et al., l992] Bodznick, D., Montgomery, J. C., and Bradley, D. J. (l992). Suppression of common mode signals within the electrosensory system of the little skate Raja erinacea. *J. Exp. Biol.*, 171:107–125.

[Chauvet, l993] Chauvet, G. A. (l993). An n-level field theory of biological neural networks. *J. Math. Biol.*, 31:771–795.

[Gerstner et al., l996] Gerstner, W., Kempter, R., van Hemmen, J. L., and Wagner, H. (l996). A neuronal learning rule for sub-millisecond temporal coding. *Nature*, 383:76–78.

[Gerstner et al., l993] Gerstner, W., Ritz, R., and van Hemmen, J. L. (l993). Why spikes? Hebbian learning and retrieval of time-resolved excitation patterns. *Biol. Cybern.*, 69:503–515.

[Gerstner and van Hemmen, l992] Gerstner, W. and van Hemmen, J. L. (l992). Associative memory in a network of 'spiking' neurons. *Network*, 3:139–164.

[Grant et al., 1998] Grant, K., Sugawara, Y., Gomes, L., Han, V., and Bell, C. C. (1998). The Mormyrid electrosensory lobe *in vitro*: Physiology and pharmacology of cells and circuits. *J. Neurosci.*, 18:6009–6025.

[Han et al., 1999] Han, V., Bell, C. C., Grant, K., and Sugawara, Y. (1999). Mormyrid electrosensory lobe in vitro: I. Morphology of cells and circuits. *J. Comp. Neurol.*, 404:359–374.

[Kempter et al., l999] Kempter, R., Gerstner, W., and van Hemmen, J. L. (l999). Symbols, neurons, soap-bubbles and the neural computation underlying cognition. *Physical Review E*, 59:4498–4514.

[Levy and Steward, 1983] Levy, W. B. and Steward, O. (1983). Temporal contiguity requirements for long-term associative potentiation/depression in the hippocampus. *Neurosci.*, 8:791–797.

[Markram et al., l997] Markram, H., Lübke, J., Frotscher, M., and Sakmann, B. (l997). Regulation of synaptic efficacy by coincidence of postsynaptic APs and EPSPs. *Science*, 275:213–215.

[Nelson and Paulin, l995] Nelson, M. E. and Paulin, M. G. (l995). Neural simulations of adaptive reafference suppression in the elasmobranch electrosensory system. *J. Comp. Physiol. A*, 177:723–736.

[Roberts, 1999a] Roberts, P. D. (1999a). Computational consequences of temporally asymmetric learning rules: I. Differential Hebbian learning. *J. Compu. Neurosci.*, 7:235–246.

[Roberts, 1999b] Roberts, P. D. (1999b). Dynamics of temporal learning rules. (submitted).

[Sejnowski, 1977] Sejnowski, T. J. (1977). Statistical constraints on synaptic plasticity. *J. Theor. Biol.*, 69:385–389.

[Zhang et al., 1998] Zhang, L. I., Tao, H. W., Holt, C. E., Harris, W. A., and ming Poo, M. (1998). A critical window for cooperation and competition among developing retinotectal synapses. *Nature*, 395:037.